

3-D Modelling of Plasticity Induced Fatigue Crack Closure- Effect of Material Constitutive Relations

Fernand Ellyin¹ and Folarin Ozah

¹ Department of Materials Engineering, The University of British Columbia,
Vancouver, B.C. Canada V6T 1Z4, e-mail: fernand@comopsites.ubc.ca

ABSTRACT. *Three-dimensional finite element method is utilized to analyze the plasticity-induced crack closure (PICC) phenomenon in a through thickness centre-cracked plate under constant amplitude cyclic loading. To accurately capture the PICC process, the choice of material model employed is of significant importance. This paper considers a relatively new model, the Ellyin-Xia elastic-plastic constitutive relations, and the more widely used kinematic hardening model. The study shows considerable difference in the results obtained while employing the two models. Experimental results support the predictions by the Ellyin-Xia material model.*

INTRODUCTION

Many researchers have investigated the crack problem in engineering structures, and various mechanisms have been identified contributing to the crack closure in these structures. These are mainly the roughness of fracture surfaces, the presence of oxides, and the development of wake plasticity. Of interest in this study is wake plasticity, which is the primary mechanism of crack closure at medium and high ΔK values [1].

Since the phenomenon of plasticity induced crack closure, PICC, was first identified by Elber [2], the finite element method has been used to model successfully the non-linear crack problem. The majority of these finite element studies consider 2-D models under plane strain and plane stress conditions, while 3-D simulations are relatively few. These 3-D crack closure studies are characterized by models that mostly employ either an elastic-perfectly-plastic, an isotropic strain hardening or a linear kinematic hardening material models for the solution of the elastic-plastic deformation. Of these, only the kinematic hardening model captures the Bauschinger effect in cyclic plasticity, which has been shown to have an important effect on the crack closure process [3, 4]. Consequently, the solutions to the non-linear crack tip fields employing the above material models vary. It is, thus, necessary to employ a material model that captures the PICC process accurately.

In this investigation, an elastic-plastic constitutive relation proposed by Ellyin and Xia [5–7] is employed as the material model for the solution of the non-linear problem subject to a constant amplitude cyclic loading. The results predicted by using this model are then compared to those obtained with the classical kinematic hardening model and experimental data.

STATEMENT OF THE PROBLEM

Although the development of wake plasticity behind the crack tip and a zone of residual compressive stress at and ahead of the crack tip at the minimum load are primary to the

PICC process, other effects of cyclic plasticity on the PICC process also need to be considered. A cracked structure undergoing cyclic plasticity at the crack tip will be strongly influenced by cyclic hardening and/or softening and by the Bauschinger effect [4] which affect the PICC process. Therefore, a material model that better describes the cyclic plastic behaviour will be of considerable value in the analysis of the crack closure mechanism. Thus, the solution to the non-linear PICC problem is dependent on the choice of the elastic-plastic constitutive relation employed for the analysis.

As stated earlier, the majority of the reported 3-D studies employ an elastic-perfectly-plastic model (no strain hardening), while a few have used an isotropic strain hardening material model. Both of these models ignore the Bauschinger effect in cyclic plasticity and thus, they over predict the crack opening level. This is because the Bauschinger effect tends to increase the plastic deformation in the reversed loading at the crack tip resulting in a reduction in the crack opening level [3, 4]. Although the kinematic hardening model considers the Bauschinger effect, there is a need to consider alternate material models that can more adequately capture the hardening or softening process associated with cyclic plasticity.

This study considers the use of a material constitutive relationship proposed by Ellyin and co-workers [5–7] which can be used to simulate quasi-static and cyclic proportional and non-proportional loading conditions while accurately capturing the effects of cyclic plasticity. This material model is used here to solve the non-linear crack problem subject to a constant amplitude cyclic loading. The kinematic hardening model provided in the ANSYS® material model library [8] is also employed for comparative purpose.

GEOMETRIC MODEL AND MESH GENERATION

In this study a through thickness centre-cracked plate subject to Mode I type cyclic loading is considered. The 3-D geometrical configuration has the following dimensions: height, $H = 80$ mm; width, $W = 80$ mm; thickness, $t = 8$ mm and an initial crack length, $2a = 8$ mm. Taking advantage of symmetry about the xy , yz and zx planes (the x -axis is along the crack plane, y -axis is perpendicular to the crack plane and the z -axis is across the plate thickness) only one eighth of the plate is modeled. The following boundary conditions are applied to the model:

$$\begin{aligned}
 u_x(0, y, z) &= 0 \rightarrow 0 \leq y \leq H/2; \quad 0 \leq z \leq t/2 \\
 u_y(x, 0, z) &= 0 \rightarrow a \leq x \leq W/2; \quad 0 \leq z \leq t/2 \\
 u_z(x, y, 0) &= 0 \rightarrow 0 \leq x \leq W/2; \quad 0 \leq y \leq H/2
 \end{aligned} \tag{1}$$

Modelling of the cracked plate employing the kinematic hardening model is accomplished using a 3-D 8-nodes structural solid, SOLID45, while the modelling of the cracked plate incorporating the Ellyin-Xia constitutive relation is achieved using a 3-D 8-nodes structural solid in the 18x family elements, SOLID185, which permits the use of the ANSYS User Programmable Features routine USERMAT.

Figure 1(a) shows a typical mesh of the model. The region away from the crack

tip consists of single layered brick elements as shown in Figure 1(a-i) with a transition to five layers through the half-thickness of the plate in the vicinity of the crack tip (see Figures 1(a-ii) and 1(a-iii)). These five layer thicknesses are chosen to match the works of Roychowdhury and Dodds Jr. [3, 9] which have layer thicknesses of $0.25t$, $0.15t$, $0.05t$, $0.03t$ and $0.02t$ where the smallest layer was located on the exterior surface of the model ($z = 0.5t$). These thicknesses allow for adequate capture of the state of stress through the half-thickness of the plate which rapidly changes from near plane strain conditions at the interior of the geometry to near plane stress conditions at the exterior surface [10–12].

The mesh has its finest refinement at the crack tip region with the smallest element length by which the crack is propagated at each cycle. The plastic zone must contain a minimum number of smallest elements to properly capture the PICC process. Therefore, a mesh refinement study was performed using crack tip element sizes: 0.08 mm, 0.04 mm, and 0.02 mm. Each mesh was checked against the adopted convergence requirement for 3-D models that at the interior surface there should be at least 5 elements in the forward plastic zone and more than one element in the reversed plastic zone. These are the plastic zone length in the plane of the crack defined by the von Mises stress attaining a value approximately equal to the yield stress of the material at the maximum and minimum load, respectively. Figures 1(b-i) and 2(b-ii) show the number of elements of size 0.02 mm elements in the forward plastic zone for the interior surface at the maximum load during the 2nd load cycle for the Ellyin-Xia model and the kinematic hardening model, respectively. By the 5th load cycle both models have a minimum of 5 elements in the forward plastic zone. In the case of the Ellyin-Xia model there were at least one or more elements than that of the kinematic model. Therefore the mesh with element size of 0.02 mm around the crack tip was used for all analyses and it consisted of 4129 elements and 5978 node with 17394 degrees of freedom.

ELASTIC-PLASTIC CONSTITUTIVE MODELS

In formulating an elastoplastic material model, three constituents are necessary [5]: (i) An initial yield criterion to specify the stress state at which plastic flow first begins; (ii) A hardening rule to specify the subsequent plastic flow as work hardening occurs; and (iii) A flow rule to relate the plastic strain-rate with the stress and stress rate.

Current incremental plasticity material models differ from each other usually with respect to the second constituent stated above, i.e. the manner in which the work hardening rule is prescribed. The various inelastic material models could be grouped under two main categories: a single surface or multi-surfaces required to describe the plastic flow. The classical isotropic and kinematic hardening rules, or their combination belong to the first group. More recent constitutive models which take into account the history of deformation fall into the second group. It is not our intention here to give a detailed review of inelastic constitutive models - it being beyond the scope of this paper. However, it will suffice to mention that the two material models used in this investigation belong to each of the above mentioned categories. An interested reader may wish to consult references [5, 13] for extensive reviews.

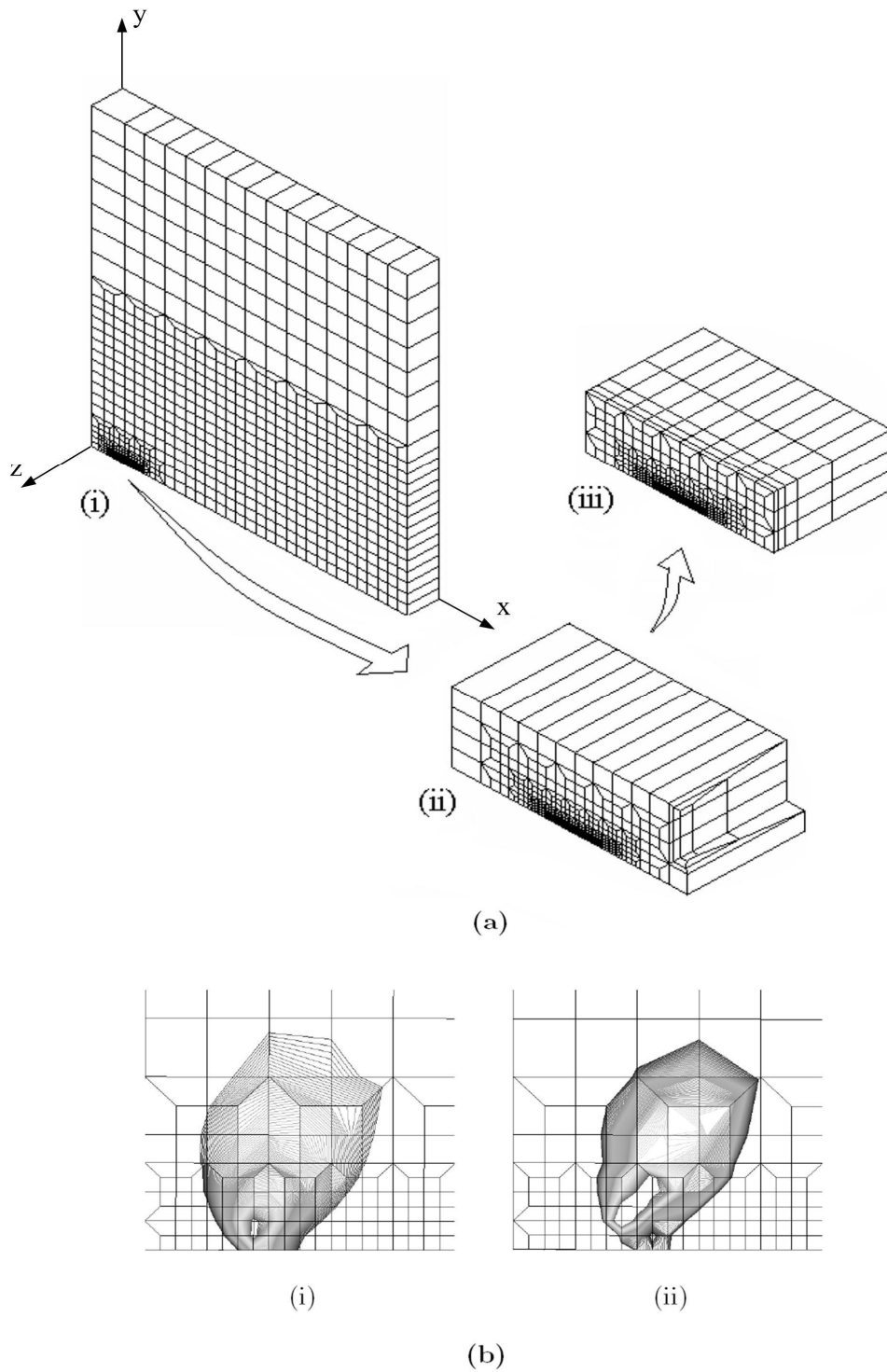


Figure 1. Mesh refinement: (a) shows how the mesh is refined with special consideration for the region around the crack tip, and (b) shows the number of elements in the forward plastic zones at the $z=0$ for the (i) Ellyin-Xia material model and (ii) kinematic hardening model at the 2nd load cycle.

FINITE ELEMENT IMPLEMENTATION

Crack Advance and Crack Surface Contact Schemes

In this study the crack is advanced at the top of the load cycle similar to previous 3-D works. The crack closure scheme was modelled similar to that used by Skinner and Daniewicz [14].

The contact scheme employed is as follows: during unloading the displacement values of the crack surface nodes were monitored, once a surface node had a negative displacement the node was constrained in the crack surface plane. After the unloading path reached the minimum load, the constraints on the surface nodes were removed before reloading.

Crack Opening Determination

The procedure defined in Wu and Ellyin [15] was employed in this study wherein a crack is considered to be open, if it has the potential to propagate. During the propagation the crack must tear through its present front to grow. The works in [10 - 12] show that the crack opening profile follows a trend in which the crack front will be the last region to have tensile stresses before the crack can grow. For this study the crack tip nodes were monitored and when the reaction force of a node became tensile that point along the front was taken as open. In order to obtain a more accurate crack opening value at the crack tip nodes each nodal reaction force was monitored for each load step and once it became tensile (positive), the zero value was obtained by linear interpolation between this tensile value and the compressive (negative) value from the previous load step.

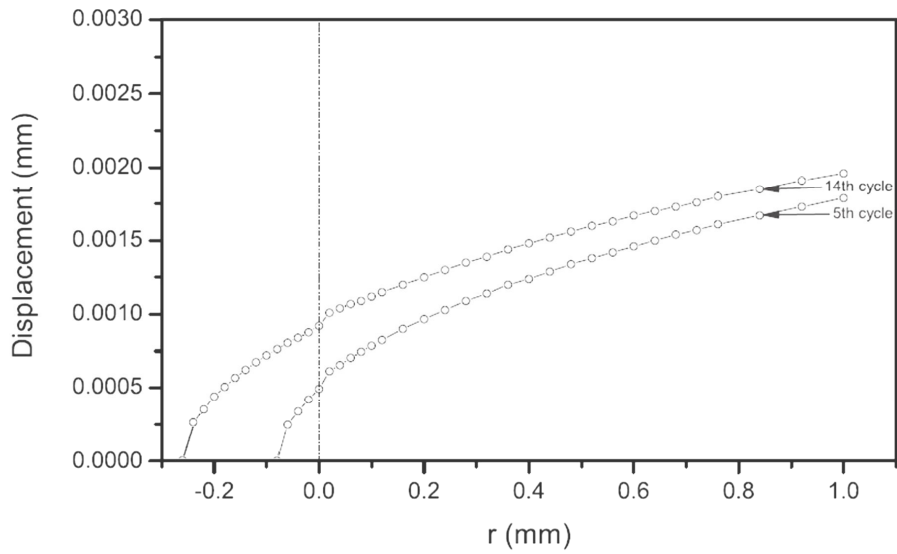
RESULTS

Crack Opening Displacement Profile

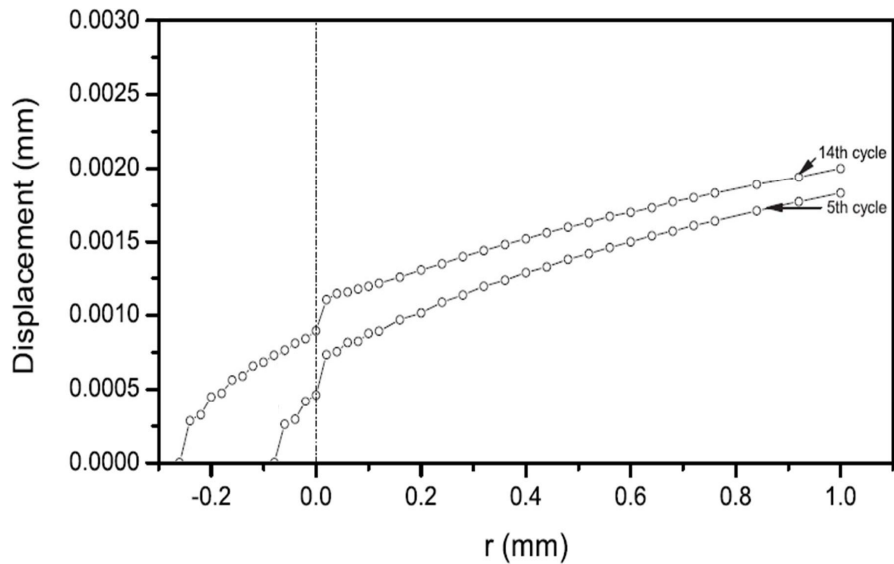
Figure 2 shows crack opening displacement profiles at the maximum applied load for the Ellyin-Xia material model (a) and kinematic hardening model (b). In these plots the initial crack tip was at the origin, $r = 0.0$. After 5 cycles the crack is advanced by four elements, $r = -0.08mm$ and after 14 cycles by $r = -0.28mm$. One notes a smoother and rounded crack tip profiles predicted by the Ellyin-Xia model in contrast to that of the kinematic hardening one. Crack tip blunting is evident in these plots, and the shape of opened crack profile does not change significantly after the 5th load cycle.

Crack Opening Stresses

Normalized crack opening values σ_{op}/σ_{max} are shown in Figure 3 for both material models employed. They indicate the expected tunneling trend of crack growth as the opening occurs first at the interior surface $z/t = 0$, then outwards to the exterior surface, $z/t = 0.50$. Although both models capture the Bauschinger effect which has been shown to result in lower opening values, the plot shows a marked difference in the through thickness stress opening values between the two models. The Ellyin-Xia material model shows a trend of lower opening values with σ_{op}/σ_{max} ratios of 0.14 at



(a)



(b)

Figure 2. Crack opening displacement profiles: (a) Ellyin-Xia Model, and (b) kinematic hardening model.

the interior ($z/t = 0$) to 0.23 at the free surface ($z/t = 0.50$) see Fig.3(b). This is in good agreement with the experimental results obtained by Craig et al. [16] which varied from 0.10 to 0.30. In contrast the dimensionless crack opening stresses varied from 0.31 to 0.38 through the thickness for the kinematic hardening model, Fig. 3(a).

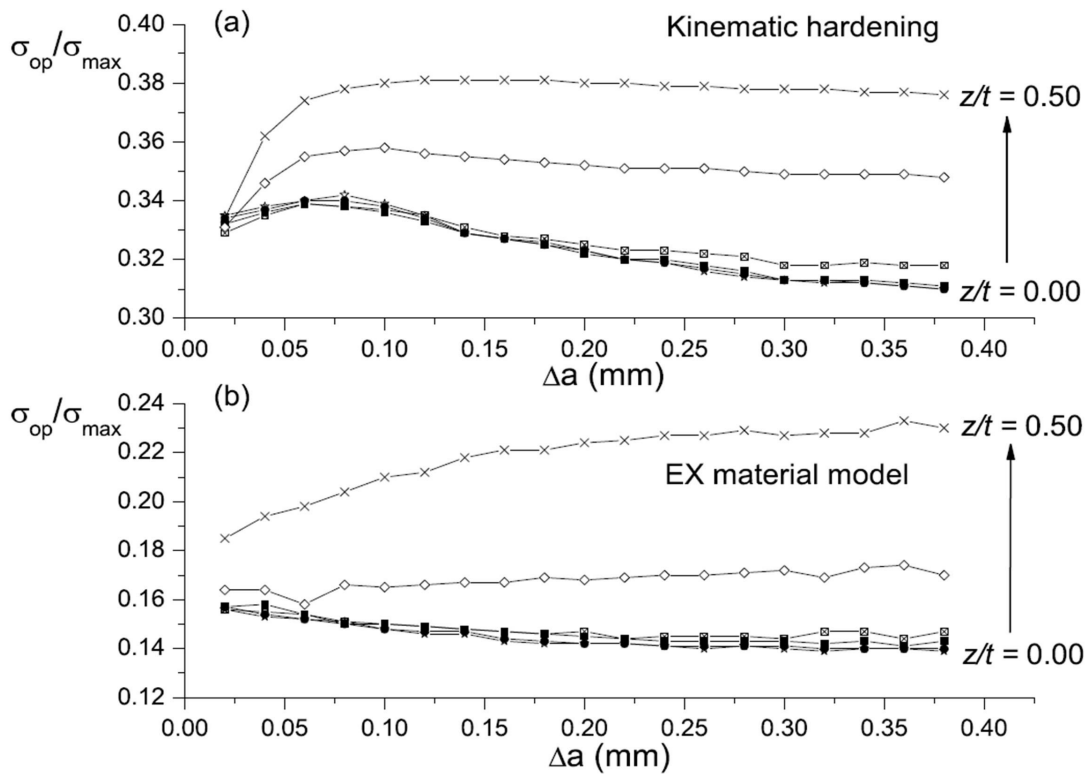


Figure 3. Normalized crack opening stress values through the thickness (interior $z/t=0$; exterior $z/t=0.5$): (a) kinematic hardening model, and (b) Ellyin-Xia model.

Reasons for this difference are as follows: Ellyin and Wu [17] have shown that classical models like the kinematic hardening do not accurately capture the unloading path of a cycle when compared to experimental results, especially in the case of variable amplitude loading histories. Also the work of Xia et al. [18] on the uniaxial cyclic loading of aluminum showed that the numerical predictions of the kinematic hardening model of the ANSYS code were not in good agreement with the experimental results. The predicted results showed a marked difference in the hysteresis loops with those of the Ellyin-Xia model being in good agreement with the experiment data.

In order to get some insight as to the reason for the difference in crack opening values, the stress and strain distributions along the crack plane will be examined below.

Stress Distribution

Figures 4(a) and 4(b) show the normalized stress distribution along the crack plane for a typical load cycle after crack opening values have been stabilized for the Ellyin-Xia and the kinematic hardening models, respectively. The profiles show the stress distribution when the crack tip is at point A; the location at which the crack opens i.e. at point 1, and at the maximum load, point 2. The crack is then advanced by an element length to point B and unloaded to point 3, the minimum load.

Since these are typical stress distribution profiles, let us consider the stress profile for the minimum load prior to point 1, which would be similar to that at point 3.

The stress profile shows that the kinematic hardening model, Fig. 4(b) predicts a larger residual compressive zone around the crack tip with a maximum value of $-\sigma_0$ throughout the thickness. In comparison the Ellyin-Xia model predicts a maximum value of $-0.25 \sigma_0$ in the interior and $-0.5 \sigma_0$ at the exterior surface. Therefore for the crack to open, the applied stress required to overcome the residual compressive zone will be higher for the kinematic model than for the Ellyin-Xia model.

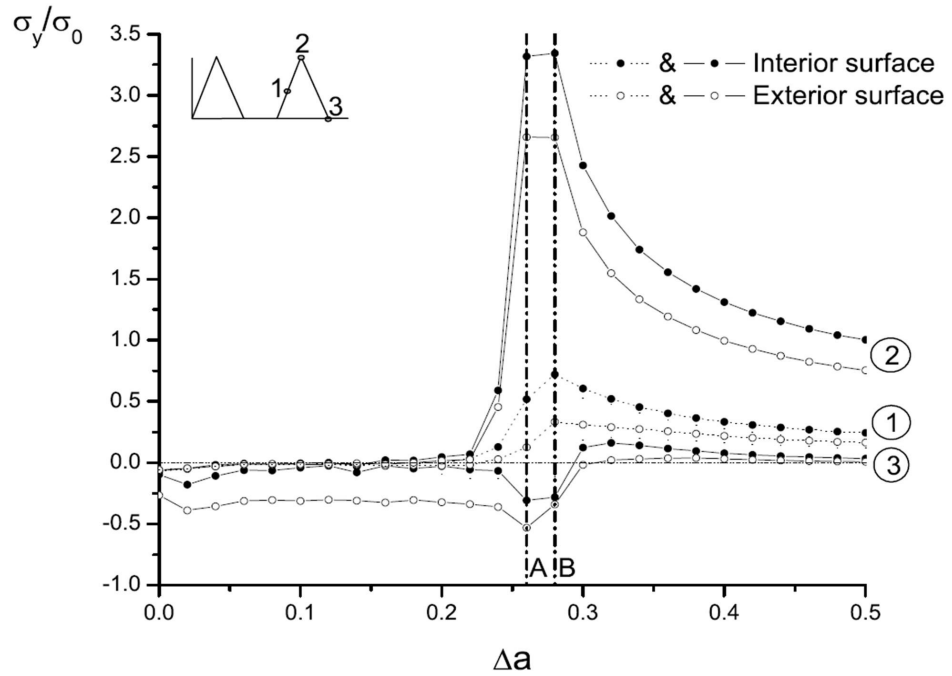
The above can be seen by examining the profiles for point 1 at which the crack opens. These profiles show higher opening values of $0.7 \sigma_0$ at the interior to $0.3 \sigma_0$ at the exterior for the Ellyin-Xia model as compared to $0.6 \sigma_0$ and $0.1 \sigma_0$, respectively for the kinematic model. At first glance it would seem that the former should have lower opening values, however, it should be noted that the total stress change from the compression (point 3), to the tension (point 1) is greater in the kinematic hardening case with the stress range values of $\Delta\sigma_y = 1.6 \sigma_0$ to $1.1 \sigma_0$ as compared to $\Delta\sigma_y = 0.95 \sigma_0$ to $0.8 \sigma_0$ for the Ellyin-Xia model.

At the maximum applied load, point 2, the stress profiles prior to the crack advance are indicated by the circular symbol 2. Although the maximum stress values for the Ellyin-Xia model are higher than those of the kinematic model at B, the stress gradient is steeper in the former resulting in lower stress values away from the crack tip. Therefore, this results in a smaller compressive zone at the minimum load as seen in the stress distribution profile for the point 3 in the Ellyin-Xia model as compared to the kinematic one. This trend is repeated for all the stabilized load cycles.

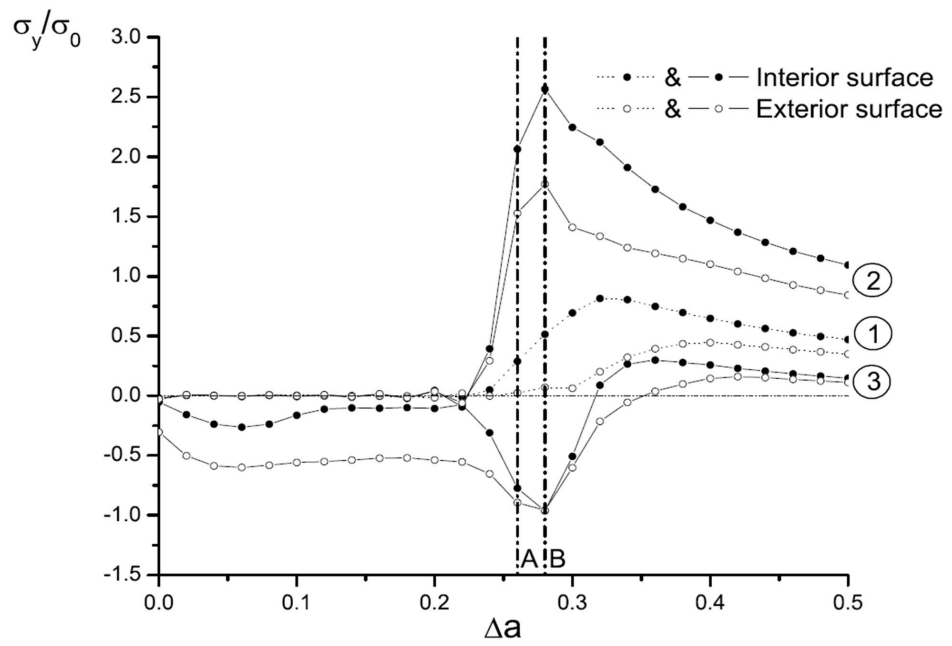
Strain Distribution

The distribution of the strain component normal to the crack plane in terms of distance from the crack tip are shown in Figs. 5(a) and 5(b) for the Ellyin-Xia and kinematic hardening models, respectively. Similar to the stress profile, the crack tip is at point A, and at the maximum load, point 2, the crack is advanced by an element length to the point B. The profile for the Ellyin-Xia model shows a smaller total change in strain, between the minimum load (point 3) and the opening one (point 1) as compared to the kinematic model. This implies more hardening in the former which would result in lower opening stresses.

As mentioned earlier the classical models like the kinematic hardening do not accurately capture the unloading path and this is where and when the Bauschinger effect is defined. Thus a material model which accurately predicts the unloading path will capture this hardening effect better, and would result in lower crack opening values.

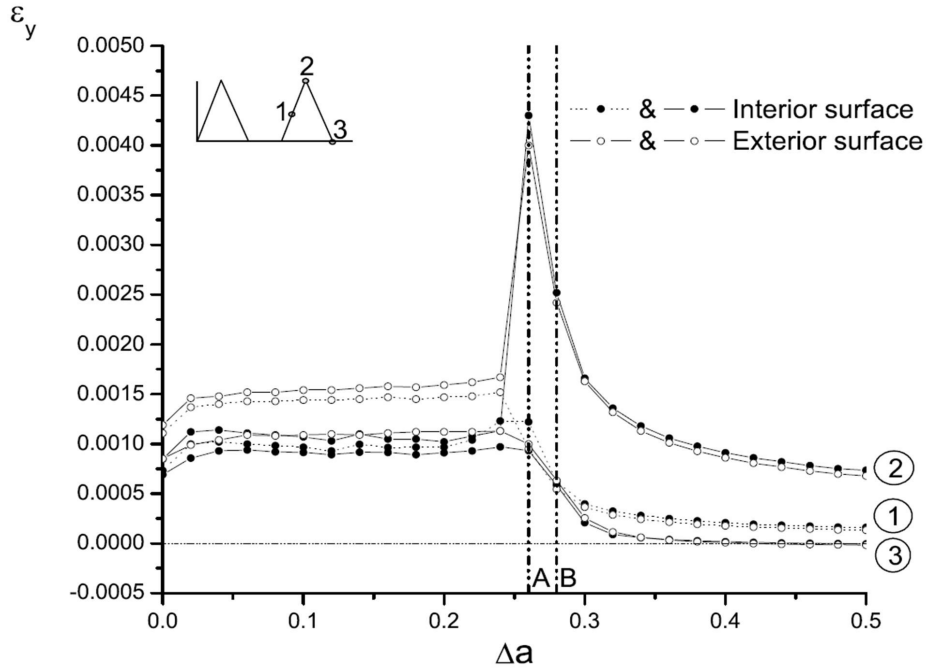


(a)

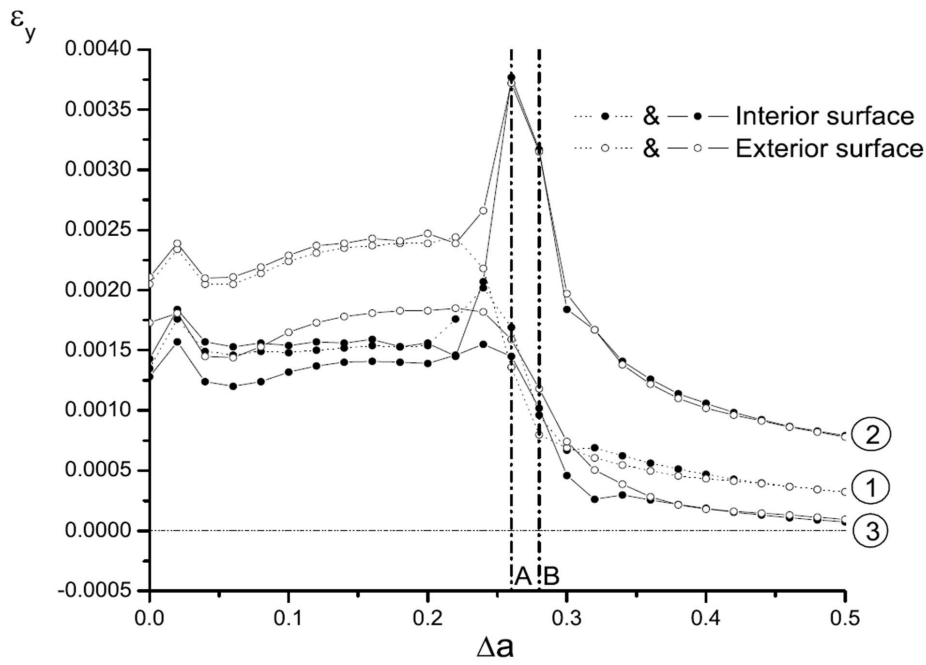


(b)

Figure 4. Stress distribution profiles: (a) Ellyin-Xia model, and (b) Kinematic hardening model.



(a)



(b)

Figure 5. Strain distribution profiles: (a) Ellyin-Xia model, and (b) Kinematic hardening model.

CONCLUSIONS

The purpose of this paper was to study the mechanics of the plasticity-induced crack closure phenomenon in a centre-cracked plate subject to a constant amplitude cyclic loading, while employing a non-linear material constitutive relation proposed by Ellyin and Xia. The results obtained with this material model were compared to those predicted by the classical kinematic hardening model.

The following conclusions were drawn from considering the crack opening stress profiles across the thickness, the stress and strain distribution profiles along the crack plane, and crack displacement profiles.

The Ellyin-Xia model shows a lower crack opening stress value as compared to the classical kinematic hardening model. This can be attributed to the way in which each model captures the unloading path in a load cycle. The classical material models do not accurately capture the unloading and reloading paths during a load cycle, while the Ellyin-Xia model captures them accurately by employing two hyper-surfaces and two types of loading regimes.

Acknowledgement

The work reported here is part of a general investigation on the fatigue and fracture of materials and structures. The research is supported, in part, by the Natural Sciences and Engineering Research Council (NSERC) of Canada through a Discovery Grant to F.E. The authors also wish to thank Dr. Yunfa Zhang for his help in revising certain figures.

REFERENCES

1. Antunes, F.V., Borrego, L. F. P., Costa, J. D. and Ferreira, J. M. (2004) *Fatigue Fract. Engng. Mater. Struct.* **27**, 825–.
2. Elber, W. (1971) *In: Damage Tolerance in Aircraft Structures*, ASTM STP 486, pp. 230–242, Amer. Soc. Testing Mater. Philadelphia, PA.
3. Roychowdhury, S. and Dodds Jr., R. H. (2003) *Engng. Fract. Mech.* **70**, 2363–2383.
4. Pommier, S. and Bompard, Ph. (2000) *Fatigue Fract. Engng. Mater. Struct.* **23**, 129–139.
5. Ellyin, F. (1997) *Fatigue Damage, Crack Growth and Life Prediction*. Chapman & Hall, London, UK.
6. Ellyin, F. and Xia, Z. (1989) *J. Mech. Phys. Solids* **37**, 71–91.
7. Ellyin, F., Xia, Z. and Wu, J. (1992) *Computers and Struct.* **56**, 189–208.
8. *ANSYS User's Manual for Revision 5.4* (1997) vol. iv Theory, ANSYS Inc., Houston, TX.
9. Roychowdhury, S. and Dodds Jr., R.H. (2003) *Fatigue Fract. Engng. Mater. Struct.* **26**, 663–673.
10. Chermahini, R.G., Shivakumar, K.N. and Newman Jr., J.C. (1988) *In: Mechanics of Fatigue Crack Closure*, ASTM STP 982, pp. 398–413, Amer. Soc. Testing Mater.

Philadelphia, PA.

11. Chermahini, R.G. and Blom, A.F. (1991) *Theo. Appl. Fract. Mech.* **15**, 267–276.
12. Chermahini, R.G., Palmberg, B. and Blom, A.F. (1993) *Int. J. Fatigue*, **15**, 259–263.
13. Lemaitre, J.(Ed.),(2001) *Handbook of Materials Behaviour Models*, in 3 volumes, Academic Press, San Diego, CA.
14. Skinner, J.D. and Daniewicz, S.R. (2002) *Engng Fract. Mech.* **69**, 1–11.
15. Wu, J. and Ellyin, F. (1996) *Int. J. Fract.* **82**, 43 – 65.
16. Craig, D., Ellyin, F. and Kujawski, D. (1995) *Fatigue Fract. Engng. Mater. Struct.* **18**, 861–873.
17. Ellyin, F. and Wu, J. (1992) *Int. J. Fract.* **56**, 189–208.
18. Xia, Z., Ellyin, F. and Meijer, G. (1997) *Compo. Sci. Technol.* **57**, 237-248.